This article has been accepted for publication in a future issue of this journal, but has not been fully edited. Content may change prior to final publication. Citation information: DOI 10.1109/TIE.2022.3159956, IEEE Transactions on Industrial Electronics

Comparative Study of Dual-Rotor Slotless Axial-Flux Permanent Magnet Machines with Equidirectional Toroidal and Conventional Concentrated Windings

Jikai Si, *Member*, *IEEE*, Tianxiang Zhang, Rui Nie, Chun Gan, *Member*, *IEEE*, and Yihua Hu, *Senior Member*

***Abstract*—Axial-flux permanent magnet (AFPM) machines are gaining popularity in low speed and high torque applications due to their high torque density, high efficiency and compact structure. In this paper, a dual-rotor slotless (DRS) AFPM (DRSAFPM) machine equipped with equidirectional toroidal winding (EDTW) is proposed and compared with that equipped with conventional single layer and double layer concentrated windings (SL and DLCWs). Firstly, the differences between the DRSAFPM machine with EDTW and that with conventional CWs in coil layout, electromotive force (EMF) and winding magnetomotive force (MMF) are revealed. Considering the special coil layout of the EDTW, the coil factor and size equations of the DRSAFPM machines with EDTW and conventional CWs are presented. Secondly, the electromagnetic performance including air-gap field, back-EMF, torque and efficiency of the DRSAFPM machines with EDTW and conventional CWs are analyzed based on the three-dimensional finite element method (3D-FEM). The simulation results validate the correctness of the coil factor and size equations and indicate the EDTW-DRSAFPM machine has superiority in back-EMF amplitude and torque density. Finally, a prototype of the EDTW-DRSAFPM machine is manufactured and tested, which validates the feasibility of the EDTW-DRSAFPM machine and the correctness of the analysis.**

***Index Terms*—Axial flux, coil factor, comparative study, concentrated windings, equidirectional toroidal windings, permanent magnet machine, size equation.**

I. Introduction

COMPARED with conventional radial-flux permanent magnet (RFPM) machines, axial-flux permanent magnet (AFPM) machines are especially suitable for direct drive low speed and high torque applications, e.g., electric and hybrid vehicles, wind turbines, flywheel energy storge system, and other applications requiring high axial space limitation due to their high torque density, high efficiency and compact structure [1-5]. In such applications, high torque density is required to satisfy working requirements, and how to further improve torque density is a hot topic that has been receiving extensive attention from researchers.

In recent years, the topologies of AFPM machines have been extensively investigated to improve the torque density, which mainly focuses on five parts: stator/rotor combination, rotor core, PM arrangements, stator core and coil layouts.

1. For the part of stator/rotor combination, the single-stator dual-rotor (TORUS type) and dual-stator single-rotor (KAMAN type) AFPM machines have been found a great interest for high torque performance applications [6]. Compared with the dual-stator single-rotor AFPM machines, the single-stator dual-rotor AFPM machines have better power density [7]. In addition, the multi-stator multi-rotor AFPM machines are made by stacking a number TORUS type or KAMAN type structures [5].

2. For the part of rotor core, its structure is investigated to improve the torque density. In [8], a novel single-stator dual-rotor AFPM machine with sinusoidal rotor segments is proposed. It is shown that the proposed machine has higher torque density than the conventional surface-mounted AFPM machines by increasing the air-gap flux density.

3. For the part of PM arrangements, the Halbach-array PM arrangement is adopted in [9], which can provide a higher flux density to increase torque density, and more sinusoidal air-gap field distribution to reduce eddy current loss.

4. For the part of stator core, the yokeless and segmented armature (YASA) single-stator dual-rotor AFPM machines are proposed in [10], [11]. It has the merits of high torque density and efficiency thanks to the high slot fill factor. In [12], [13], the cooling systems of the YASA machines are investigated to improve the power and torque density.

5. For the part of coil layouts, several studies have shown that AFPM machines with distributed windings have difficulties in finding suitable space for the long and bulky inner end-windings [14]. Compared with the distributed windings, concentrated windings are gaining popularity in AFPM machines due to their short end-windings, low copper loss and

This work is partially supported by National Natural Science Foundation of China under grant No.51777060, in part by the Major Special Project for Collaborative Innovation in Zhengzhou No. 20XTZX12023. (Corresponding author: Tianxiang Zhang)

Jikai Si, Tianxiang Zhang and Rui Nie are with the Zhengzhou University, Zhengzhou, 450001, China (e-mail: sijikai@zzu.edu.cn; zhangtianxiang@gs.zzu.edu.cn; nierui@zzu.edu.cn).

Chun Gan is with the Huazhong University of Science and Technology, Wuhan, 430074, China (e-mail: chungan@hust.edu.cn).

Yihua Hu is with the University of York, York, YO105DD, UK (e-mail: yihua.hu@york.ac.uk).

This article has been accepted for publication in a future issue of this journal, but has not been fully edited. Content may change prior to final publication. Citation information: DOI 10.1109/TIE.2022.3159956, IEEE Transactions on Industrial Electronics

simple winding structure. The single-layer and double-layer concentrated windings and toroidal windings used in single-stator dual-rotor or dual-stator single-rotor AFPM machines are investigated in [15], [16]. It is shown that the single-layer concentrated winding (SLCW) has higher torque capability due to its higher coil factor compared with the double-layer concentrated winding (DLCW) in certain circumstances. The toroidal winding requires 16 % less copper compared with the single-layer concentrated winding with the same torque performance in certain slot/pole/phase combination.

As an extension of the study about winding configurations, an equidirectional toroidal winding (EDTW) is proposed in [17], [18] by our research team, which are used in RFPM machines. Different from the conventional windings, only the positive sides of the coils are left on one side of the stator core, the return sides of the coils are all removed to the other side of the stator core. To present the features of the EDTW, Fig. 1 shows the RFPM machines with SLCW, DLCW and EDTW. The meanings of the EDTW are: (1) The winding direction of all coils is identical. (2) All the coils of each phase have the same positive current direction. (3) All the coils in a phase have the identical instantaneous current direction on one side of the stator core due to the special coil layout of the EDTW, which is shown in Fig. 1(c) (Different from the EDTW, the coils of conventional concentrated windings in a phase have different instantaneous current direction due to there are both positive and return sides of the coils on one side of the stator core, which are shown in Fig. 1(a), (b)).

It is demonstrated that the RFPM machines with EDTW have higher torque capability [17], [18]. Nevertheless, the machine which is proposed in [17] has the disadvantages of high torque ripple and low winding utilization rate. It could be expected that the EDTW is suitable for the single-stator dual-rotor AFPM machines, which could take full advantage of the EDTW. In addition, the slotless structure is adopted for a smooth operation due to its merit of zero-cogging compared with slotted structure [19]. Therefore, a dual-rotor slotless (DRS) AFPM (DRSAFPM) machine equipped with EDTW is proposed and compared with that equipped with conventional SL and DLCWs in this paper, the former has the same total number of coils as the EDTW, while the latter has the same number of coils on one side of the stator core as the EDTW.

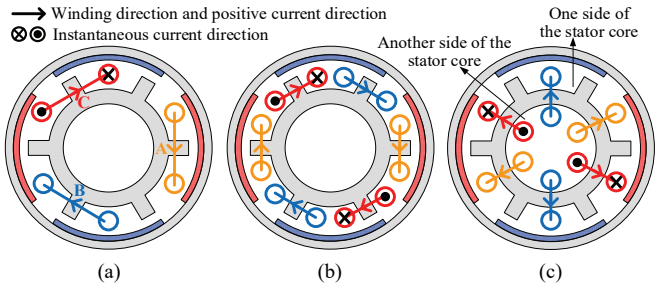

Fig. 1. RFPM machines with (a) SLCW. (b) DLCW. (c) EDTW.

The main contributions of this paper are: (1) Proposing an EDTW structure used in DRSAFPM machine to improve the torque density. (2) Revealing the differences between the DRSAFPM machines with conventional CWs and those with EDTW in terms of the coil layout, operational principle, coil factor, and size equations. Introducing the conductor factor K_{c2} to represents the discount of the vector sum of the EMF of all the conductors per phase compared to their algebraic sum. (3) Presenting a comprehensive comparative study of the DRSAFPM machines with conventional CWs and those with EDTW in electromagnetic performance. (4) Manufacturing and testing the prototype of the EDTW-DRSAFPM machine.

II. Machine Structure and Operation Principle

A. Machine Structure and Coil Layout

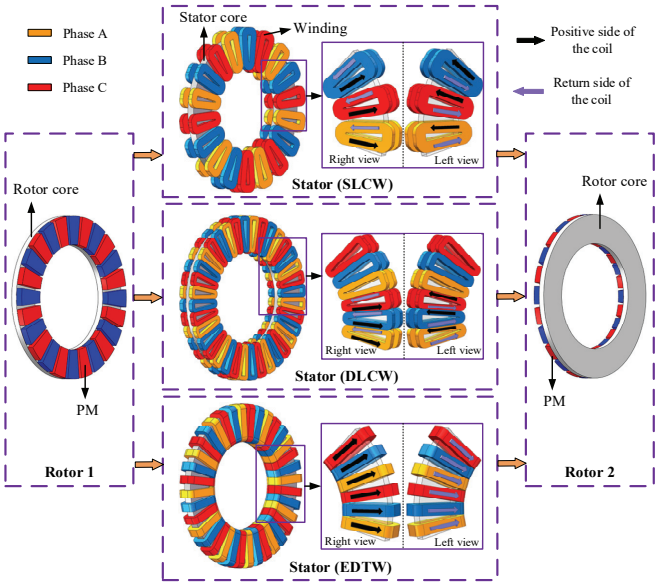

Fig. 2. DRSAFPM machines with SLCW, DLCW and EDTW.

Fig. 2 shows the topology of DRSAFPM machines with SLCW, DLCW and EDTW, respectively. It is shown that the structure is similar to the conventional TORUS type machines, including two rotors and one stator which is sandwiched in between. The three machines differ only in their winding types. As can be seen, for the conventional CWs, there are both positive and return sides of the coils on one side of the stator core. Different from the conventional CWs, for the EDTW, there are only positive sides of the coils (A+, B+ and C+) on one side of the stator core, and the return sides of the coils (A-, B- and C-) are all removed to the other side of the stator core. To illustrate the operation principle of the EDTW-DRSAFPM machine and clarify the difference between the DRSAFPM machines with conventional CWs and those with EDTW, the electromotive force (EMF) and winding magnetomotive force (MMF) of the three machines will be analyzed below.

B. Electromotive Force

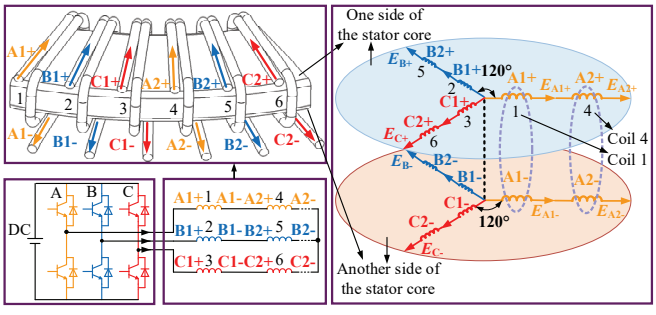

Fig. 3. Three-phase coil-EMF vector on both sides of the stator core and winding connection of the 1/6 model of the EDTW-DRSAFPM machine.

This article has been accepted for publication in a future issue of this journal, but has not been fully edited. Content may change prior to final publication. Citation information: DOI 10.1109/TIE.2022.3159956, IEEE Transactions on Industrial Electronics

Fig. 3 shows the three-phase coil-EMF vector and the winding connection of the 1/6 model of the EDTW-DRSAFPM machine (six coils, two pole pairs). It is shown that the incoming line terminals (A1+, B1+ and C1+) are connected to a three-phase power source, the outcoming line terminals (A2-, B2- and C2-) are connected in wye connection. Due to the special coil layout of the EDTW, the coil-EMF of the positive sides of the coils (E_{A+}, E_{B+}, and E_{C+}) are all on one side of the stator core, and the coil-EMF of the return sides of the coils (E_{A-}, E_{B-}, and E_{C-}) are all on the other side of the stator core.

To further clarify the features of the EDTW, the three-phase coil-EMF vector of the 1/6 models of the SLCW- (three coils, two pole pairs), DLCW- (six coils, two pole pairs) and EDTW-DRSAFPM machines on one side of the stator core are analyzed and compared, which are shown in Fig. 4. The electrical radian of one coil is defined as coil pitch θ_p, and the electrical radian between the middle of the coil band is θ_b. The w_c is the width of the coil band. The R_o and R_i are the outer radius and inner radius of the stator, respectively. The θ_{co} and θ_{ci} are the electrical radians of one coil band at R_o and R_i, respectively. When the influence of the coil band on the EMF is ignored, the peak phase-EMF of one coil side can be expressed as

$$E_1=\pi B_g N_1 \frac{f}{p}\left(R_o^2-R_i^2\right) \tag{1}$$

where, B_g is the peak value of the air-gap flux density, f is the machine frequency, N_1 is the turns per coil, p is the pole pairs.

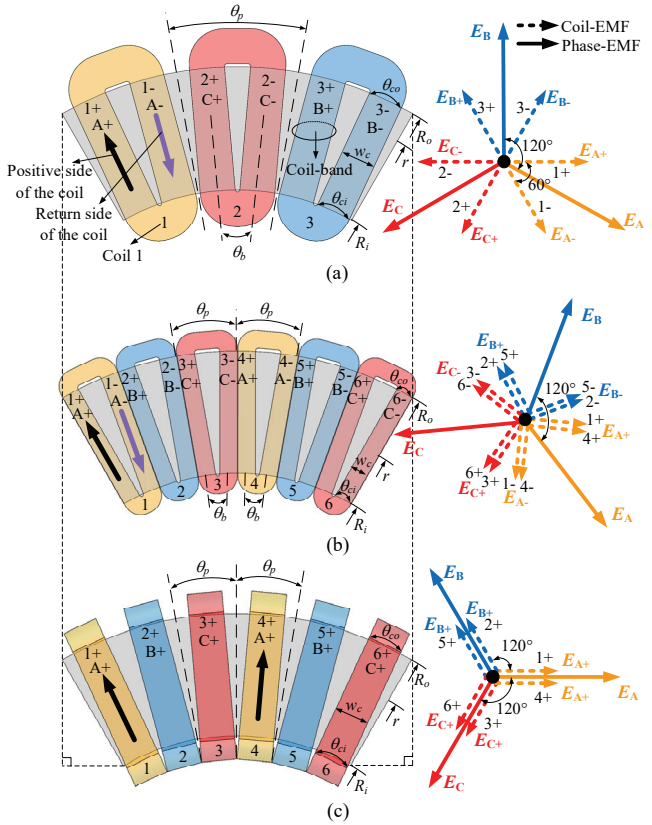

Fig. 4. Coil layouts and three-phase coil-EMF vector diagram of the 1/6 model of the three machines on one side of the stator core. (a) SLCW-DRSAFPM. (b) DLCW-DRSAFPM. (c) EDTW-DRSAFPM.

As shown in Fig.4, the phase-EMF (e.g., E_A shown in Fig. 4(a)) of the DRSAFPM machines with conventional CWs are both synthesized by the coil-EMF of the positive (e.g., E_{A+} shown in Fig. 4(a)) and return (e.g., E_{A-} shown in Fig. 4(a)) sides of the coils. There are phase differences between the coil-EMF of positive and return side of one coil. The coefficient to represent the reduction in the synthetic phase-EMF due to the phase differences could be called pitch factor. Therefore, the peak phase-EMF of the conventional CWs can be defined as

$$E_{CW}=2\pi B_g N_{ph} \frac{f}{p}\left(R_o^2-R_i^2\right)\underbrace{\sin\left(\theta_b/2\right)}_{k_p} \tag{2}$$

where, N_{ph} is the number of turns per phase, k_p is the pitch factor.

However, for the EDTW-DRSAFPM machine, the phase-EMF (e.g., E_A shown in Fig. 4(c)) is only synthesized by the coil-EMF of the positive sides of the coils (e.g., two E_{A+} shown in Fig.4 (c)). Similarly, on the other side of the stator core, the phase-EMF of the EDTW-DRSAFPM machine is only synthesized by the coil-EMF of the return sides of the coils, which means the coil-EMF of the positive and return sides of the coils does not contribute to each other. It can be considered that the pitch factor of the EDTW-DRSAFPM machine is always 0.5. Therefore, the peak phase-EMF of the EDTW can be defined as

$$E_{EDTW}=\pi B_g N_{ph} \frac{f}{p}\left(R_o^2-R_i^2\right)=2\pi B_g N_{ph} \frac{f}{p}\left(R_o^2-R_i^2\right)\underbrace{0.5}_{k_p} \tag{3}$$

In a brief summary, the differences between the DRSAFPM machines with conventional CWs and those with EDTW in coil layout and EMF are as follows

1) For the DRSAFPM machines with conventional CWs, there are both positive and return sides of the coils on one side of the stator core, and the phase-EMF are synthetic by the coil-EMF of the positive and return sides of the coils.
2) For the DRSAFPM machine with EDTW, only positive or return sides of the coils are left on one side of the stator core, and the phase-EMF are only synthetic by the coil-EMF of the positive or return sides of the coils.

C. *Winding Magnetomotive Force*

Fig. 5 shows the winding magnetomotive force (MMF) of the minimum unit of the conventional CWs and EDTW on one side of the stator core when only phase A is energized. The one-side minimum unit of the SLCW-DRSAFPM machine contains three coils and two pole pairs, but that of the DLCW- and EDTW-DRSAFPM machines both contains three coils and one pole pair. The MMF of one coil side can be expressed as

$$F_1=\frac{N_1 i}{\pi}\sum_v \frac{1}{v}\sin v\left(\theta_m-\psi\right) \tag{4}$$

where, i is the current, v is the MMF space harmonic order, θ_m is the angular measure around the air gap, ψ is the mechanical radians from zero reference point.

As can be seen, on one side of the stator core, the A-phase MMF of the conventional CWs are both produced by the positive and return sides of the coils, which are shown in Fig. 5(a), and Fig. 5(b), respectively. Hence, the A-phase MMF of the minimum unit of the conventional CWs can be expressed as

$$\begin{aligned} F_{A\text{-}CW}\left(\theta_m\right)&=\frac{N_{ph} i}{\pi}\sum_v \frac{1}{v}\left[\sin v\left(\theta_m-\psi\right)-\sin v\left(\theta_m-\psi-\theta_b/p_0\right)\right] \\ &=\frac{2N_{ph} i}{\pi}\sum_v \frac{1}{v}\cos v\left(\theta_m-\psi-\theta_b/2p_0\right)\underbrace{\sin v\theta_b/\left(2p_0\right)}_{k_p} \end{aligned} \tag{5}$$

where, p_0 is the pole pairs of the minimum unit, k_p is the pitch factor of the v-th harmonic, which represents the reduction in

This article has been accepted for publication in a future issue of this journal, but has not been fully edited. Content may change prior to final publication. Citation information: DOI 10.1109/TIE.2022.3159956, IEEE Transactions on Industrial Electronics

the A-phase MMF due to the phase differences between the positive and return sides of the coil.

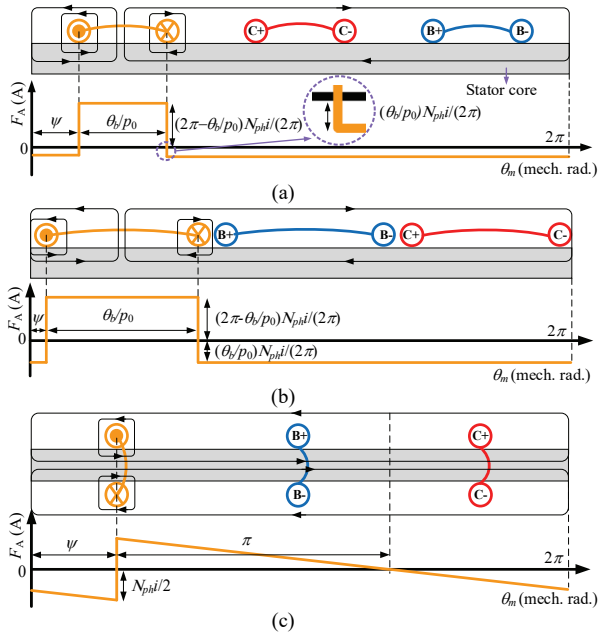

Fig. 5. A-phase winding MMF of the minimum unit of the three winding types on one side of the stator core. (a) SLCW. (b) DLCW. (c) EDTW.

However, the A-phase MMF of the EDTW is only produced by the positive side of the coil on one side of the stator core, which is shown in Fig. 5(c). Hence, the A-phase MMF of the minimum unit of the EDTW can be defined as

$$F_{A\text{-EDTW}}(\theta_m)=\frac{N_{ph}i}{\pi}\sum_v\frac{1}{v}\sin v(\theta_m-\psi)=\frac{2N_{ph}i}{\pi}\sum_v\frac{1}{v}\sin v(\theta_m-\psi)\underbrace{0.5}_{k_p} \quad (6)$$

Different from the conventional CWs, the pitch factor of the EDTW is always 0.5. It could be expected that the MMF of the other phase windings are similar to the A-phase MMF of the respective winding types, only in different current and positions. The three phase currents are defined as

$$\begin{cases} i_A(t)=I\cos(\omega t+\varphi) \\ i_B(t)=I\cos(\omega t+\varphi-2\pi/3) \\ i_C(t)=I\cos(\omega t+\varphi+2\pi/3) \end{cases} \quad (7)$$

where, the ω is the angular frequency, t is the time, φ is the initial phase angle, I is the peak value of the current. The A-, B- and C-phase MMF variation against t and θ_m of the minimum unit of the conventional CWs can be expressed as

$$\begin{cases} F_{A\text{-CW}}(t,\theta_m)=\dfrac{2N_{ph}I}{\pi}\cos(\omega t+\varphi) \\ \quad\times\sum_v\dfrac{1}{v}\cos v(\theta_m-\psi-\theta_b/2p_0)\underbrace{\sin v\theta_b/(2p_0)}_{k_p} \\ F_{B\text{-CW}}(t,\theta_m)=\dfrac{2N_{ph}I}{\pi}\cos(\omega t+\varphi-2\pi/3) \\ \quad\times\sum_v\dfrac{1}{v}\cos v(\theta_m-\psi-\theta_b/2p_0-2\pi/3)\underbrace{\sin v\theta_b/(2p_0)}_{k_p} \\ F_{C\text{-CW}}(t,\theta_m)=\dfrac{2N_{ph}I}{\pi}\cos(\omega t+\varphi+2\pi/3) \\ \quad\times\sum_v\dfrac{1}{v}\cos v(\theta_m-\psi-\theta_b/2p_0-4\pi/3)\underbrace{\sin v\theta_b/(2p_0)}_{k_p} \end{cases} \quad (8)$$

The A-, B- and C-phase MMF variation against t and θ_m of the minimum unit of the EDTW can be expressed as

$$\begin{cases} F_{A\text{-EDTW}}(t,\theta_m)=\dfrac{2N_{ph}I}{\pi}\cos(\omega t+\varphi) \\ \quad\times\sum_v\dfrac{1}{v}\sin v(\theta_m-\psi)\underbrace{0.5}_{k_p} \\ F_{B\text{-EDTW}}(t,\theta_m)=\dfrac{2N_{ph}I}{\pi}\cos(\omega t+\varphi-2\pi/3) \\ \quad\times\sum_v\dfrac{1}{v}\sin v(\theta_m-\psi-2\pi/3)\underbrace{0.5}_{k_p} \\ F_{C\text{-EDTW}}(t,\theta_m)=\dfrac{2N_{ph}I}{\pi}\cos(\omega t+\varphi+2\pi/3) \\ \quad\times\sum_v\dfrac{1}{v}\sin v(\theta_m-\psi-4\pi/3)\underbrace{0.5}_{k_p} \end{cases} \quad (9)$$

Therefore, the three-phase MMF variation against t and θ_m of the minimum unit of the conventional CWs that of the EDTW can be expressed as

$$\begin{cases} F_{\text{CW}}(t,\theta_m)=F_{A\text{-CW}}(t,\theta_m)+F_{B\text{-CW}}(t,\theta_m)+F_{C\text{-CW}}(t,\theta_m) \\ F_{\text{EDTW}}(t,\theta_m)=F_{A\text{-EDTW}}(t,\theta_m)+F_{B\text{-EDTW}}(t,\theta_m)+F_{C\text{-EDTW}}(t,\theta_m) \end{cases} \quad (10)$$

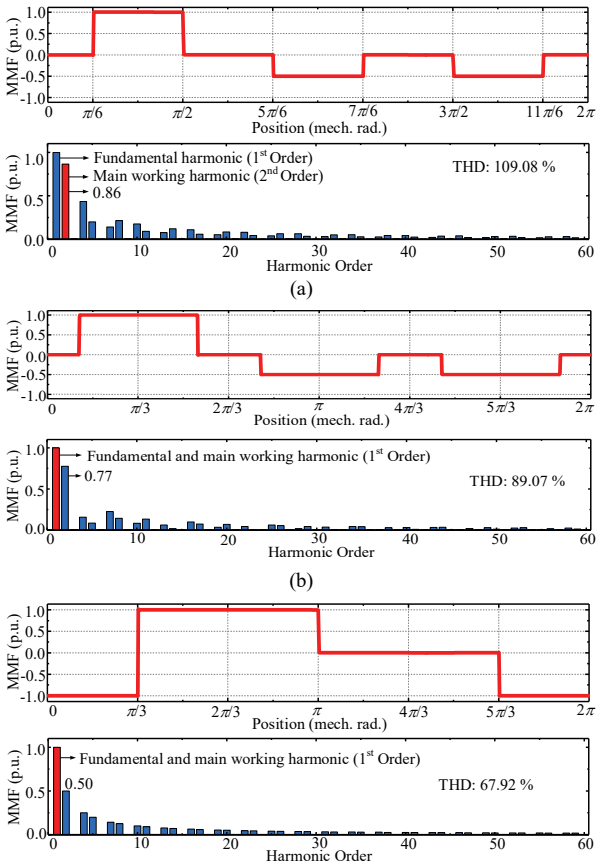

Fig. 6. There-phase winding MMF and its harmonics spectra of the minimum unit of the conventional CWs and EDTW on one side of the stator core. (a) SLCW. (b) DLCW. (c) EDTW.

According to Equation (8)-(10), the three-phase winding MMF and its harmonic spectra of the minimum unit of the conventional CWs and EDTW on one side of the stator core can be obtained, which are shown in Fig. 6. It could be observed that the fundamental and main working harmonics of the DLCW and EDTW are both 1st, which equal the number of

This article has been accepted for publication in a future issue of this journal, but has not been fully edited. Content may change prior to final publication. Citation information: DOI 10.1109/TIE.2022.3159956, IEEE Transactions on Industrial Electronics

corresponding pole pairs. The fundamental harmonic of the stator winding MMF are normally highest and as the main working harmonic to match the rotor pole pairs. However, this condition is not valid for all winding types [20]. As shown in Fig. 6(a), the fundamental and main working harmonics of the winding MMF of the SLCW are 1st and 2nd, respectively.

The differences between the DRSAFPM machines with conventional CWs and those with EDTW in winding MMF on one side of the stator core are summarized as follows

1) Each phase winding MMF of the conventional CWs are both produced by the positive and return sides of the coils, but that of the EDTW is only produced by the positive or return sides of the coils.
2) The fundamental and main working harmonics of the three-phase winding MMF of the DLCW and EDTW are both 1st. However, for the SLCW, the fundamental harmonic is 1st and the main working harmonic is 2nd.

III. Coil Factor and Size Equations

A. Coil Factor

Owing to the special coil layout of the EDTW, the coil factor of the DRSAFPM machines with conventional CWs and EDTW should be analyzed and compared. For the conventional CWs, the pitch factor should be considered. Additionally, in slotless AFPM machines, the width of the coil band should also be considered. There would be a reduction of the EMF vector sum since the conductors in one coil band are not in phase, and the coefficient to represent the reduction is called band factor [21]. The coil factor of the conventional CWs is influenced by pitch factor and band factor. However, for the EDTW, the pitch factor is always 0.5, which is explained in the previous section. Therefore, the magnitude of the coil factor of the EDTW is only determined by band factor.

The premise of the calculation is that the conductors in one coil band are evenly distributed, and they are symmetric to the middle of the coil band. The band factor $k_b(r)$ can be expressed as [21]

$$k_b(r)=\frac{2r}{pw_c}\sin\left(pw_c/2r\right) \tag{11}$$

For the SLCW-DRSAFPM machine, the θ_b does not change at different radii r. Hence, the pitch factor of the SLCW-DRSAFPM machine ($k_{p\text{-SLCW}}$) is

$$k_{p\text{-SLCW}}=\sin\left(\theta_b/2\right) \tag{12}$$

For the DLCW-DRSAFPM machine, the θ_b changes at different radii r. Therefore, the pitch factor of the DLCW-DRSAFPM machine ($k_{p\text{-DLCW}}(r)$) can be expressed as

$$k_{p\text{-DLCW}}(r)=\sin\left[\theta_p/2-pw_c/(2r)\right] \tag{13}$$

Therefore, the coil factor of the SLCW-DRSAFPM machine ($k_{c\text{-SLCW}}$) can be defined as

$$\begin{aligned}k_{c-\text{SLCW}}&=\frac{\int_{R_i}^{R_o}\left(B\cdot\Omega\cdot r\cdot k_b(r)\cdot k_{p-\text{SLCW}}\right)dr}{\int_{R_i}^{R_o}\left(B\cdot\Omega\cdot r\right)dr}\\&=\frac{\sin\left(\frac{\theta_b}{2}\right)}{3\left(\frac{1}{\theta_{co}^2}-\frac{1}{\theta_{ci}^2}\right)}\left\{\frac{4}{\theta_{co}^3}\sin\left(\frac{\theta_{co}}{2}\right)+\frac{1}{\theta_{co}^2}\cos\left(\frac{\theta_{co}}{2}\right)\right.\\&\quad-\frac{1}{2\theta_{co}}\sin\left(\frac{\theta_{co}}{2}\right)-\frac{4}{\theta_{ci}^3}\sin\left(\frac{\theta_{ci}}{2}\right)\\&\quad-\frac{1}{\theta_{ci}^2}\cos\left(\frac{\theta_{ci}}{2}\right)+\frac{1}{2\theta_{ci}}\sin\left(\frac{\theta_{ci}}{2}\right)\\&\quad\left.+\frac{1}{4}\left[\text{Ci}\left(\frac{\theta_{co}}{2}\right)-\text{Ci}\left(\frac{\theta_{ci}}{2}\right)\right]\right\}\end{aligned} \tag{14}$$

where, B is the air-gap flux density, Ω is the mechanical angular velocity of the machine.

The coil factor of the DLCW-DRSAFPM machine ($k_{c\text{-DLCW}}$) can be expressed as

$$\begin{aligned}k_{c\text{-DLCW}}&=\frac{\int_{R_i}^{R_o}\left[B\cdot\Omega\cdot r\cdot k_b(r)\cdot k_{p\text{-DLCW}}(r)\right]dr}{\int_{R_i}^{R_o}\left(B\cdot\Omega\cdot r\right)dr}\\&=\frac{1}{3\left(\frac{1}{\theta_{co}^2}-\frac{1}{\theta_{ci}^2}\right)}\left\{\left(\frac{2}{\theta_{co}^3}-\frac{1}{\theta_{co}}\right)\cos\left(\frac{\theta_p}{2}-\theta_{co}\right)-\left(\frac{2}{\theta_{ci}^3}-\frac{1}{\theta_{ci}}\right)\right.\\&\quad\times\cos\left(\frac{\theta_p}{2}-\theta_{ci}\right)+\frac{1}{\theta_{co}^2}\sin\left(\frac{\theta_p}{2}-\theta_{co}\right)\\&\quad-\frac{1}{\theta_{ci}^2}\sin\left(\frac{\theta_p}{2}-\theta_{ci}\right)+\left[\text{Ci}(\theta_{co})-\text{Ci}(\theta_{ci})\right]\\&\quad\times\sin\left(\frac{\theta_p}{2}\right)-\left[\text{Si}(\theta_{co})-\text{Si}(\theta_{ci})\right]\cos\left(\frac{\theta_p}{2}\right)\\&\quad\left.+\left(\frac{2}{\theta_{ci}^3}-\frac{2}{\theta_{co}^3}\right)\cos\left(\frac{\theta_p}{2}\right)\right\}\end{aligned} \tag{15}$$

The coil factor of the EDTW-DRSAFPM machine ($k_{c\text{-EDTW}}$) can be defined as

$$\begin{aligned}k_{c-\text{EDTW}}&=\frac{\int_{R_i}^{R_o}\left[B\cdot\Omega\cdot r\cdot k_b(r)/2\right]dr}{\int_{R_i}^{R_o}\left(B\cdot\Omega\cdot r\right)dr}\\&=\frac{1}{6\left(\frac{1}{\theta_{co}^2}-\frac{1}{\theta_{ci}^2}\right)}\left\{\frac{4}{\theta_{co}^3}\sin\left(\frac{\theta_{co}}{2}\right)+\frac{1}{\theta_{co}^2}\cos\left(\frac{\theta_{co}}{2}\right)\right.\\&\quad-\frac{1}{2\theta_{co}}\sin\left(\frac{\theta_{co}}{2}\right)-\frac{4}{\theta_{ci}^3}\sin\left(\frac{\theta_{ci}}{2}\right)\\&\quad-\frac{1}{\theta_{ci}^2}\cos\left(\frac{\theta_{ci}}{2}\right)+\frac{1}{2\theta_{ci}}\sin\left(\frac{\theta_{ci}}{2}\right)\\&\quad\left.+\frac{1}{4}\left[\text{Ci}\left(\frac{\theta_{co}}{2}\right)-\text{Ci}\left(\frac{\theta_{ci}}{2}\right)\right]\right\}\end{aligned} \tag{16}$$

where

This article has been accepted for publication in a future issue of this journal, but has not been fully edited. Content may change prior to final publication. Citation information: DOI 10.1109/TIE.2022.3159956, IEEE Transactions on Industrial Electronics

$$\begin{cases} \theta_{ci} = \left(p \cdot w_c\right) / R_i \\ \theta_{co} = \left(p \cdot w_c\right) / R_o \\ \mathrm{Si}(x) = \int_0^x \dfrac{\sin u}{u} du = \sum_{n=0}^{\infty} \dfrac{(-1)^n}{(2n+1)(2n+1)!} x^{2n+1} \\ \mathrm{Ci}(x) = \int_{\infty}^x \dfrac{\cos u}{u} du = \gamma + \ln x + \sum_{n=1}^{\infty} \dfrac{\left(-x^2\right)^n}{(2n)(2n)!} \end{cases} \tag{17}$$

In conclusion, the differences between the DRSAFPM machines with conventional CWs and those with EDTW in coil factor are summarized as follows

1) For the DRSAFPM machine with conventional CWs, the coil factor is both influenced by pitch factor and band factor. The pitch factor of the SLCW-DRSAFPM machine does not change at different radii *r*, but that of the DLCW-DRSAFPM machine changes at different radii *r*.
2) For the DRSAFPM machine with EDTW, the pitch factor is always 0.5, the magnitude of coil factor is only influenced by band factor.

The coil factor equations of the three DRSAFPM machines are analyzed in this part, especially the EDTW-DRSAFPM machine, which could help to calculate the coil factor of the EDTW-DRSAFPM machine, and then help to analyze the performance of the machine, such as back-EMF, power and torque, etc.

B. Size Equations

The rotor on both sides of the AFPM machines are symmetrical, hence, they could be designed according to the structure of single stator and single rotor. If the stator leakage inductance and resistance are neglected, the output power P_{out} of the single side AFPM machines can be expressed as [22]

$$P_{out} = \eta \frac{m}{T} \int_0^T e(t) i(t) \mathrm{d}t = \eta m K_p E_{pk} I_{pk} \tag{18}$$

where, η is the machine efficiency, m is the number of phases of the machine, T is the period of one cycle of the EMF, $e(t)$ is the phase EMF, $i(t)$ is the phase current, K_p is the electrical power waveform factor, I_{pk} is the peak value of the phase current, E_{pk} is the peak value of the phase EMF.

According to the Equation (2) and (3), the E_{pk} of the single side DRSAFPM machines can be expressed as

$$E_{pk} = \frac{\pi}{2} K_c N_{ph} B_g \frac{f}{p} \left(1 - K_r^2\right) D_o^2 \tag{19}$$

where, K_c is the coil factor, K_r is the ratio of inner to outer diameter of the stator core, D_o is the outer diameter of the stator core.

It should be noted that the number of turns per phase N_{ph} of the DRSAFPM machines with conventional concentrated windings (the N_{ph} of the SLCW and DLCW are the same) and EDTW are different. Fig. 7 shows the 1/6 model of the two machines with conventional CW (take the SLCW as an example) and EDTW. The premise is that the number of conductors per phase N_c of the two machines on one side of the stator core are identical. For the SLCW, on one side of the stator core, the N_{ph} is 2 (shown in Fig. 7(a)), which is the half of the number of conductors per phase N_c (N_{ph}=N_c/2). For the EDTW, the N_{ph} is 4 (shown in Fig. 7(b)), which equal the N_c (N_{ph}=N_c). The electric loading of the single side DRSAFPM machines with CWs and EDTW can be expressed as

$$A_{\mathrm{CW}} = 2mN_{ph}I_{rms} / \left(\pi D_{avg}\right) \tag{20}$$

$$A_{\mathrm{EDTW}} = mN_{ph}I_{rms} / \left(\pi D_{avg}\right) \tag{21}$$

where, I_{rms} is the Root-Mean-Square (RMS) of the phase current, D_{avg} is the average value of the inner and outer diameters of the stator core.

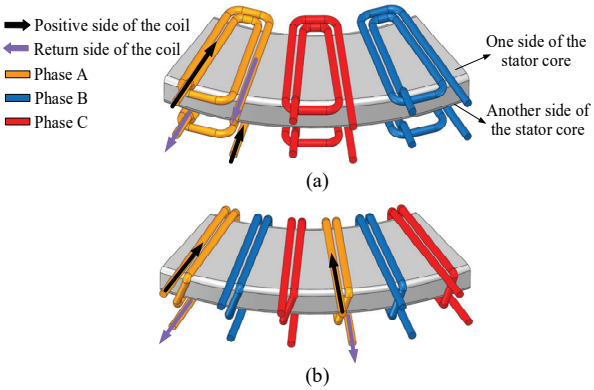

Fig. 7. 1/6 model of the two machines with SLCW and EDTW. (a) SLCW. (b) EDTW.

The peak value of the phase current of the single side DRSAFPM machines with conventional CWs and EDTW can be obtained from Equation (20) and (21), and as shown below

$$I_{pk\text{-CW}} = \sqrt{2}\pi A_{\mathrm{CW}} \left(1 + K_r\right) D_o / \left(4mN_{ph}\right) \tag{22}$$

$$I_{pk\text{-EDTW}} = \sqrt{2}\pi A_{\mathrm{EDTW}} \left(1 + K_r\right) D_o / \left(2mN_{ph}\right) \tag{23}$$

According to Equation (18)-(23), the output power of the single side DRSAFPM machines with conventional CWs and EDTW can be expressed as

$$P_{out\text{-CW}} = \frac{\sqrt{2}}{8} \pi^2 \eta K_p K_c B_g A_{\mathrm{CW}} \frac{f}{p} \left(1 - K_r^2\right)\left(1 + K_r\right) D_o^3 \tag{24}$$

$$P_{out\text{-EDTW}} = \frac{\sqrt{2}}{4} \pi^2 \eta K_p K_c B_g A_{\mathrm{EDTW}} \frac{f}{p} \left(1 - K_r^2\right)\left(1 + K_r\right) D_o^3 \tag{25}$$

The output torque of the single side DRSAFPM machines with conventional CWs and EDTW can be expressed as

$$T_{out\text{-CW}} = \frac{\sqrt{2}}{16} \pi \eta K_p K_c B_g A_{\mathrm{CW}} \left(1 - K_r^2\right)\left(1 + K_r\right) D_o^3 \tag{26}$$

$$T_{out\text{-EDTW}} = \frac{\sqrt{2}}{8} \pi \eta K_p K_c B_g A_{\mathrm{EDTW}} \left(1 - K_r^2\right)\left(1 + K_r\right) D_o^3 \tag{27}$$

It is shown that the size equations of the AFPM machines with conventional CWs and EDTW are different due to the N_{ph} of the DRSAFPM machines with CWs is half the N_c, but that of the DRSAFPM machine with EDTW equal the N_c. In addition, the coil factor K_c of the DRSAFPM machine with EDTW is 0.5 maximum due to the features of the toroidal winding. However, the K_c of the DRSAFPM machines with conventional CWs is 1 maximum. The N_{ph} of the DRSAFPM machine with EDTW is twice that of the DRSAFPM machines with conventional CWs when the N_c of the DRSAFPM machines with conventional CWs and EDTW is identical. According to Equation (19), it is hard to intuitively compare the back-EMF capability of the DRSAFPM machines with conventional CWs and EDTW through the coil factor K_c. Therefore, it is necessary to analyze how to make size equations of the DRSAFPM machines with conventional CWs and EDTW expressed uniformly and

compared intuitively.

If the N_{ph} is replaced by the N_c, the Equation (19) for the conventional CWs and EDTW could be rewritten as

$$E_{pk\text{-CW}} = \frac{\pi}{4} N_c B_g \frac{f}{p}\left(1-K_r^2\right) D_o^2 \underbrace{K_c}_{K_{c2}} \tag{28}$$

$$E_{pk\text{-EDTW}} = \frac{\pi}{4} N_c B_g \frac{f}{p}\left(1-K_r^2\right) D_o^2 \underbrace{2K_c}_{K_{c2}} \tag{29}$$

where, K_{c2} is defined as conductor factor, which represents the discount of the vector sum of the EMF of all the conductors per phase compared to their algebraic sum. It is shown that the K_{c2} of the DRSAFPM machines with conventional CWs equal the K_c (K_{c2}= K_c), but that of the DRSAFPM machine with EDTW is twice the K_c (K_{c2}=2K_c). When the N_{ph} is replaced by N_c, the Equation (20) and (21) for the conventional CWs and EDTW could be expressed uniformly

$$A = mN_c I_{rms} / \left(\pi D_{avg}\right) \tag{30}$$

The peak value of the phase current of the single side DRSAFPM machines can be obtained from Equation (30), and as shown below

$$I_{pk} = \sqrt{2}\pi A\left(1+K_r\right) D_o / \left(2mN_c\right) \tag{31}$$

According to Equation (18), (28)-(31), the output power of the single side DRSAFPM machines with conventional CWs and EDTW can be expressed uniformly by introducing the concept of the conductor factor K_{c2}, and as expressed

$$P_{out} = \frac{\sqrt{2}}{8}\pi^2 \eta K_p K_{c2} B_g A \frac{f}{p}\left(1-K_r^2\right)\left(1+K_r\right) D_o^3 \tag{32}$$

The output torque of the single side DRSAFPM machines with conventional CWs and EDTW can be expressed as

$$T_{out} = \frac{\sqrt{2}}{16}\pi\eta K_p K_{c2} B_g A\left(1-K_r^2\right)\left(1+K_r\right) D_o^3 \tag{33}$$

In conclusion, the differences between the DRSAFPM machines with conventional CWs and those with EDTW in size equations are summarized as follows

1) The N_{ph} of the DRSAFPM machines with conventional CWs is half the N_c. However, for the EDTW-DRSAFPM machine, the N_{ph} equals the N_c, which means that the N_{ph} of the EDTW-DRSAFPM machine is higher than that of the DRSAFPM machines with conventional CWs, when the N_c of the DRSAFPM machines with conventional CWs and EDTW are identical.
2) For the DRSAFPM machines with conventional CWs, the K_{c2} equals the K_c. Nevertheless, the K_{c2} of the EDTW-DRSAFPM machine is twice the K_c.

According to the analysis of the differences between the DRSAFPM machine with conventional CWs and EDTW in size equations, the size equations which are suitable for the EDTW-DRSAFPM machine are proposed. Such size equations could help to initial design the parameters of the EDTW-DRSAFPM machine when the performances requirements are given, and help to quickly predict the performances of the EDTW-DRSAFPM machine when the parameters of the machine are given. In addition, when the machine is optimized, the parameters before and after the machine optimization through the size equations can be quickly analyzed and compared.

C. Key Parameters Determination

The rated output power and speed of the whole machine of the design requirements are 2.2 kW and 400 rpm, respectively. Therefore, the rated output power and torque of the single side EDTW-DRSAFPM machine are 1.1 kW and 26.3 Nm. The EDTW-DRSAFPM machine could be designed with more pole pairs due to the large radial size of the AFPM machines, which has the benefits of low inductive reactance, high power factor and high efficiency. Considering the low speed of the proposed EDTW-DRSAFPM machine, 12 pole pairs are selected and the frequency is 80 Hz. Therefore, the number of coils of the EDTW-DRSAFPM machine should be 36.

For the AFPM machines, the ratio of inner to outer of the stator core K_r is a very important parameter. Generally, values of K_r that optimize torque density are to be found in the 0.65 to 0.75 range [5]. At the same time, the output torque should also be considered. In this paper, the preliminary design of K_r is 0.65. According to Equation (32) and (33), the outer diameter of stator core D_o is related to the magnetic loading and electric loading. For the magnetic loading, the remanence B_r of the N48SH is about 1.36 T, the maximum magnetic energy product B_g/B_r is about 0.5. Therefore, the air-gap flux density B_g is about 0.68 T. For the electric loading, the electric loading A is related to the loss and structure parameters and allowable temperature rise ΔT of the machine. The A at the average radius of the air cooling AFPM machines is generally 16-32 kA/m [5]. In this paper, considering the allowable temperature rise, the A is about 29.5 kA/m.

According to Equation (32) and (33), the outer diameter of the stator core D_o could be obtained, which is about 234 mm. Considering that the outer diameter of the total machine is limited to 260 mm, the output toque should be as high as possible, and the length of winding protrude should also be considered, the D_o takes 240 mm in this paper. Therefore, the inner diameter of the stator core D_i is 156 mm and the average diameter of the stator core D_{avg} is 198 mm.

Owing to the driver current limitation (12 Arms), the requirement of rated current is 10 Arms. According to the Equation (30), the number of conductors per phase of the EDTW-DRSAFPM machine could be obtained, which is about 612. So far, the main parameters of the machine have been determined, and the design method of the rest parameters is basically the same as that of the conventional radial machine, which could be refer to the [23].

The design preconditions of the DRSAFPM machines with conventional CWs and EDTW are as below

1) The main dimensions of the three machines are identical.
2) The three machines have the similar total number of conductors on each side of the stator core.

Briefly, the electric and magnetic loadings of the three machines are basically the same. According to the design preconditions, the main parameters of the SLCW-, DLCW- and EDTW-DRSAFPM machines are listed in TABLE I.

IV. Electromagnetic Performance

Based on the parameters of the three machines listed in TABLE I, the three-dimensional (3D) models of the three machines are established and their characteristics are analyzed by 3D-FEM in this section. To reduce simulation time and improve efficiency, the solution space is chosen by means of

This article has been accepted for publication in a future issue of this journal, but has not been fully edited. Content may change prior to final publication. Citation information: DOI 10.1109/TIE.2022.3159956, IEEE Transactions on Industrial Electronics

symmetric boundary conditions.

TABLE I
MAIN PARAMETERS OF THE THREE DRSAFPM MACHINES

Parameters	SLCW-DRSAFPM	DLCW-DRSAFPM	EDTW-DRSAFPM
Rated speed	400 rpm	400 rpm	400 rpm
Rated current I_{rms}	10 A	10 A	10 A
Number of pole pairs p	12	12	12
Number of phase m	3	3	3
Total coils	36	72	36
One-side coils	18	36	36
Turns per coil N_1	51	25	51
Turns per phase N_{ph}	306	300	612
Conductors per phase N_c	612	600	612
Electric loading A	29.52 kA/m	28.94 kA/m	29.52 kA/m
Outer radius of stator R_o	120 mm	120 mm	120 mm
Inner radius of stator R_i	78 mm	78 mm	78 mm
Coil band width w_c	12 mm	6 mm	12 mm
Winding thickness	7 mm	7 mm	7 mm
Air-gap length	1 mm	1 mm	1 mm
Axial length	58 mm	58 mm	58 mm
Phase resistance @ 60℃	1.48 Ω	1.23 Ω	1.44 Ω

A. Air-Gap Field

The air-gap fields produced by PM MMF (PM fields) of the three machines in the range of 60 mechanical degrees (1/6 model, two pole pairs) are shown in Fig. 8. The three machines differ only in their winding structure, hence, the PM fields of the three machines are similar. It can be seen that, for each machine, the major PM field harmonic is 2nd, which equals the number of pole pairs of the PMs in the range of 60 mechanical degrees. In addition, the amplitudes of 2nd harmonic of the SLCW-, DLCW-, EDTW-DRSAFPM machines are all 0.77 T.

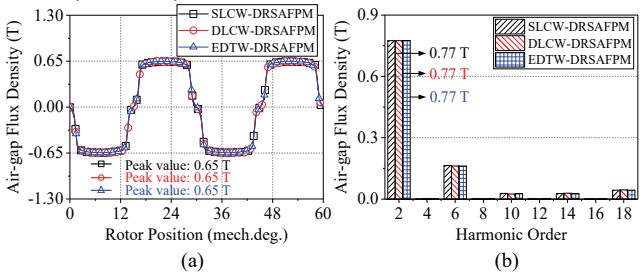

Fig. 8. Comparison of air-gap fields produced by PM MMF of the three machines. (a) Waveforms. (b) Harmonic spectra.

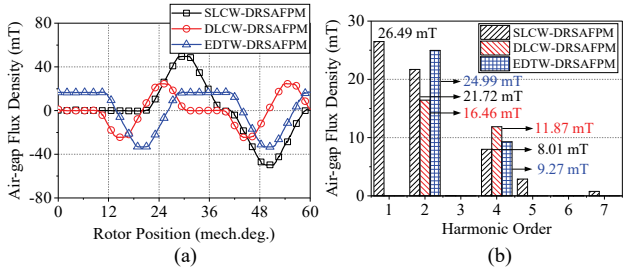

Fig. 9. Comparison of air-gap fields produced by winding MMF of the three machines. (a) Waveforms. (b) Harmonic spectra.

The air-gap fields produced by winding MMF (armature fields) of the three machines in the range of 60 mechanical degrees (1/6 models) are shown in Fig. 9 (i_a=0 A, i_b=-5$\sqrt{3}$ A and i_c=5$\sqrt{3}$ A). The 1/6 model of the SLCW-DRSAFPM consists of 1 minimum unit (three coils and two pole pairs on one side), and the 1/6 models of the DLCW- and EDTW-DRSAFPM machine consist of 2 minimum units (six coils and two pole pairs on one side). Therefore, the main working armature field harmonics of the three machines are all 2nd, which equal the major PM field harmonic in the range of 60 mechanical degrees. Compared with the SLCW and DLCW-DRSAFPM machines, the amplitude of the major armature field harmonic (2nd) of the EDTW-AFDRPSM machine is increased by 15.06 % and 51.82 %, respectively.

B. No-Load Back-EMF Characteristics

According to the Equation (28) and (29), the fundamental harmonic phase back-EMF of the DRSAFPM machines can be defined as

$$E_f = \frac{\pi}{2} N_c B_f \frac{f}{p} (1 - K_r^2) D_o^2 K_{c2} \tag{34}$$

where, B_f is the fundamental harmonic air-gap flux density.

As shown in TABLE I and Fig. 8, it can be concluded that the results of other parameters except K_{c2} in the Equation (34) are basically the same. According to Equation (14)-(16), the coil factor and conductor factor of the three machines could be obtained, as shown in TABLE II. It is shown that the fundamental harmonic conductor factor of the SLCW-, DLCW- and EDTW-DRSAFPM machines are 0.79, 0.62 and 0.91, respectively. If the other parameters except K_{c2} of the Equation (34) of the three machines are the same, which means the fundamental back-EMF of the EDTW-DRSAFPM machine is theoretically 15.19 % and 46.77 % higher than that of the SLCW- and DLCW-DRSAFPM machines, respectively.

TABLE II
COIL FACTOR AND CONDUCTOR FACTOR OF THE THREE MACHINES

Harmonic order	Coil factor		
	SLCW-DRSAFPM	DLCW-DRSAFPM	EDTW-DRSAFPM
1st	0.79	0.62	0.46 (0.457)
2nd	0.59	0.89	0.34
3rd	0	0.71	0.19
	Conductor factor		
1st	0.79	0.62	0.91 (0.914)
2nd	0.59	0.89	0.68
3rd	0	0.71	0.38

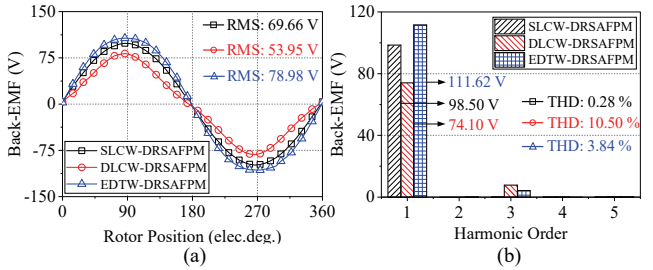

Fig. 10. Comparison of no-load back-EMF of the three machines. (a) Waveforms. (b) Harmonic spectra.

Fig. 10 presents the comparison of no-load back-EMF waveform and its harmonics spectra of the three machines at rated speed (400 rpm). As shown in Fig. 10(b), the amplitude of back-EMF fundamental harmonic of the EDTW-DRSAFPM machine (111.62 V) is 13.32 % and 50.63 % higher than that of the SLCW- (98.50 V) and DLCW-DRSAFPM (74.10 V) machines, respectively, which validate the correctness of the coil factor and size equations. The reasons for the slight differences between the simulation and theory are that the different total number of conductors of the three machines and the different errors between the calculated and simulated back-EMF of the three machines, which will be explained later. In addition, the total harmonic distortion (THD) of no-load back-

This article has been accepted for publication in a future issue of this journal, but has not been fully edited. Content may change prior to final publication. Citation information: DOI 10.1109/TIE.2022.3159956, IEEE Transactions on Industrial Electronics

EMF of the SLCW-, DLCW- and EDTW-DRSAFPM machines are 0.28 %, 10.50 % and 3.84 %, respectively.

According to the Equation (34), the fundamental harmonic no-load back-EMF variation against speed of the three machines can be obtained, which is shown in Fig. 11. It should be noted that the B_f needs to be considered as the average value of fundamental harmonic air-gap flux density in the axial range of windings of the three machines. As can be seen, the trends of the calculated results and 3D finite element analysis (3D-FEA) results are basically consistent, which further validate the correctness of the coil factor and size equations. The calculated and simulated fundamental back-EMF of the three machines at rated speed are summarized in TABLE III. It is shown that there are errors between the calculated and simulated back-EMF and the errors of the three machines are different. The reasons are that the neglect of the PM field edge effect and the ignorance of the influence of leakage flux at the end windings on back-EMF. It should be noted the influence of leakage flux at the end windings on back-EMF of the three machines are different due to the different type and length of the end windings, which lead to the different errors of the three machines.

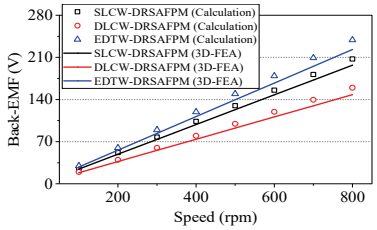

Fig. 11. Fundamental harmonic of no-load back-EMF variation against speed of the three machines.

TABLE III
CALCULATED AND SIMULATED FUNDAMENTAL BACK-EMF OF THE THREE MACHINES AT RATED SPEED

Back-EMF	SLCW-DRSAFPM	DLCW-DRSAFPM	EDTW-DRSAFPM
Calculation	103.74 V	79.82 V	119.50 V
3D-FEA	98.50 V	74.10 V	111.62 V
Related error	5.32 %	7.72 %	7.07 %

C. *On-Load Torque Characteristics*

Fig. 12 shows the torque performances of the three machines at rated current (RMS: 10 A). As shown in Fig. 12(a), the torque-current angle indicates the relative angle between the current phasor and *d*-axis. It is shown that all the machines achieve maximum torque when the torque-current angle is 90 elec. deg. (I_d=0). The rated torque waveforms of the three machines are shown in Fig. 12(b). In conclusion, compared with the SLCW- and DLCW-DRSAFPM machines, the total torque density of the EDTW-DRSAFPM machine is increased by 12.59 % and 47.23 % without dramatic aggravation of the torque ripple.

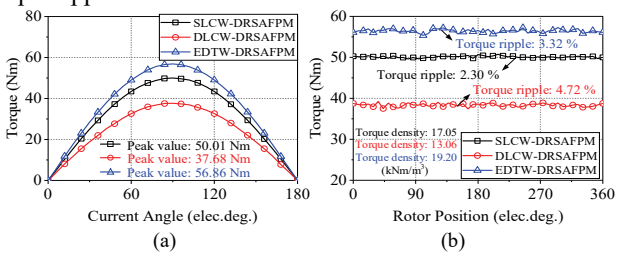

(a) (b)

Fig. 12. Torque performances of the three machines at rated current. (a) Torque-current angle characteristic. (b) Rated torque waveforms.

D. *Loss and Efficiency*

Fig. 13 shows the loss and efficiency of the three machines. It should be noted that the excitation source of loss and efficiency analysis is the current source, without limiting terminal voltage and ignoring the influence of flux-weakening. As can be seen from Fig. 13(a), within the whole speed region, the core loss and PM loss of the SLCW-DRSAFPM machine are always higher than those of the DLCW- and EDTW-DRSAFPM machines. That is caused by the abundant armature field harmonic content of the SLCW, which is shown in Fig. 9(b). The efficiency of the three machines is shown in Fig. 13(b). As can be seen, within the whole speed region, the efficiency of the EDTW-DRSAFPM machine is higher than that of the SLCW- and DLCW-DRSAFPM machines, thanks to the improved output torque/power. The loss and efficiency at rated working point are listed in TABLE IV. For the low-speed and high-torque applications, the copper loss of the DRSAFPM machines accounted for a major proportion of the total loss. It is shown that the rated efficiency of the EDTW-DRSAFPM machine is 84.45 %, which is 2.41 % and 3.32 % higher than that of the SLCW- and DLCW-DRSAFPM machine, respectively.

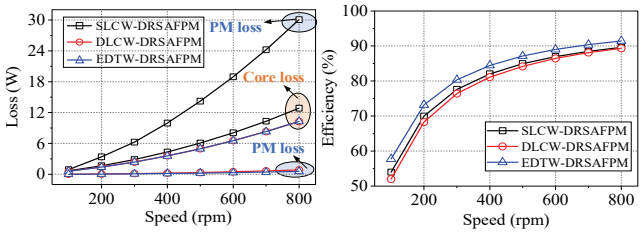

(a) (b)

Fig. 13. Loss and efficiency variation against speed of the three machines. (a) Loss. (b) Efficiency.

TABLE IV
LOSS AND EFFICIENCY AT RATED WORKING POINT

	SLCW-DRSAFPM	DLCW-DRSAFPM	EDTW-DRSAFPM
Effective copper loss	258.89 W	258.89 W	258.89 W
End-winding cooper loss	186.49 W	111.25 W	172.59 W
Copper loss	445.38 W	370.14 W	431.48 W
Core loss	4.33 W	3.59 W	3.57 W
PM loss	9.96 W	0.23 W	0.15 W
Output power	2099.47 W	1607.42 W	2364.11 W
Efficiency	82.04 %	81.13 %	84.45 %

E. *Flux-Weakening Characteristics*

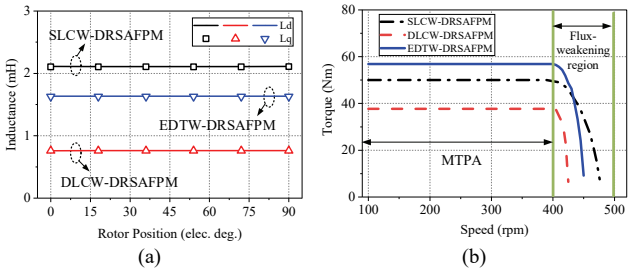

(a) (b)

Fig. 14. Flux-weakening performance of the three machines. (a) Inductances. (b) Torque versus speed.

When considering the output voltage limit of the inverter, the flux-weakening performance of the machines should be considered after the machines' speed exceeds the rated speed. Below the rated speed, the torque is kept at its rated value. The region is called the Maximum Torque Per Ampere region (MTPA) [24]. Above the rated speed, the *d*-axis

This article has been accepted for publication in a future issue of this journal, but has not been fully edited. Content may change prior to final publication. Citation information: DOI 10.1109/TIE.2022.3159956, IEEE Transactions on Industrial Electronics

demagnetization current is increased that the armature field counter-acts the PM field. The region is called flux-weakening region. Fig. 14 shows the flux-weakening performance of the three machines. It is shown that the poor flux-weakening capabilities of the three machines are obvious. For the slotless surface mounted AFPM machines, the inductance values are low due to the large effective air gaps in the machines' magnetic circuit, which is limited to lower the magnet flux linkage [25]. Therefore, it causes limits on the DRSAFPM machines' constant-power region during flux-weakening operation.

V. Experimental Validation

To verify the analyses aforementioned, a prototype of the EDTW-DRSAFPM machine is manufactured, which is shown in Fig. 15. The detailed manufactured process is illustrated as below.

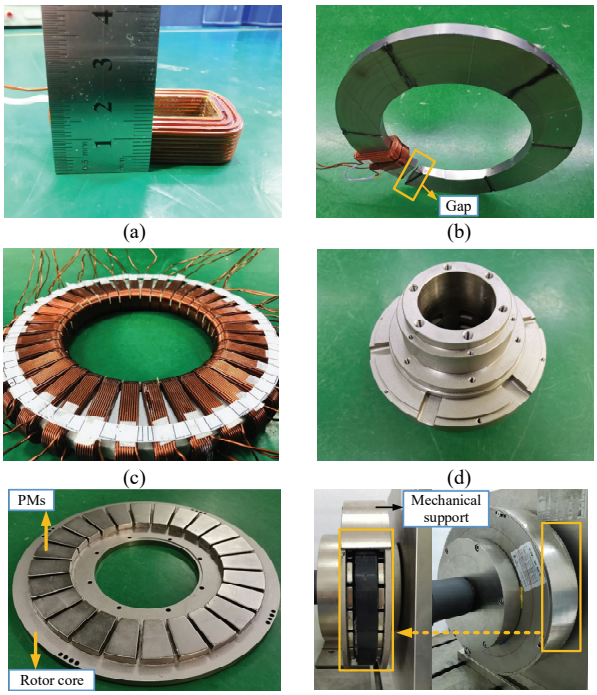

Fig. 15. Prototype of the EDTW-DRSAFPM machine. (a) Toroidal winding. (b) Stator core. (c) Stator. (d) Shaft. (e) Rotor. (f) Prototype.

1. Stator core and windings: Fig. 15 (a) shows a toroidal winding, which is wound by winding machine and manufactured separately. The windings are kept in shape by brushing epoxy. The stator core is slotless structure, which is made of spirally wound 50WW310 silicon steel sheet. For the DRSAFPM machines with conventional concentrated windings, the concentrated windings are easy to assemble, which could directly paste on the stator core. However, for the EDTW-DRSAFPM machine, the assembly of toroidal winding is more complicated. In this processing scheme, a gap is left on the stator core, and the toroidal windings are set on the stator core from the gap, which is shown in Fig. 15(b). The toroidal windings are fixed with the stator core by epoxy and the gap is welded after assembly. Fig. 15(c) shows the assembled stator, all the positive sides of the coils are on one side of the stator core, the return sides of the coils are all on the other side of the stator core.

2. Rotor core and PMs: The DRSAFPM machine proposed in this paper is the surface-mounted PM machine. Therefore, the PMs are directly sticked to the rotor core, which is shown in Fig 15(e). The materials of the PMs are N48SH. The rotor core is solid and its material is steel-1010, which is consistent with the 3D-FEA. The outer diameter of the rotor core extends outward to facilitate the connection of the two rotors, and the inner diameter of the rotor core extends inward to facilitate connection with the bearing.

3. Prototype assembly: Fig 15(d) shows the shaft. The stator and shaft are encapsulated together by epoxy. The two rotors are connected with shaft by two bearings, which could assure the air-gap length. In addition, the two rotors of the prototype are connected each other by two mechanical supports, and one rotor is connected to the load, which is shown in Fig. 15(f).

It can be summarized that there are some manufacturing difficulties in toroidal windings assembly, two rotors connection and air-gap length assurance of the EDTW-DRSAFPM prototype. In our processing scheme, the detailed toroidal winding assembly method has been mentioned in the stator core and winding part, the two rotors are connected by mechanical supports, and the air-gap length is assured by two bearings. Nevertheless, it is still difficult to ensure the accurate parameters of the prototype due to the machining accuracy.

The prototype testing platform is shown in Fig. 16. It is shown that the prototype testing platform consists of the prototype of the EDTW-DRSAFPM machine, magnetic powder brake, drive motor, torque transducer (4503A200L00B1000 Kistler), power analyzer (WT5000 Yokogawa), oscilloscope (DL850E Yokogawa), driver (SERVOTRONIX CDHD), loading controller and computer.

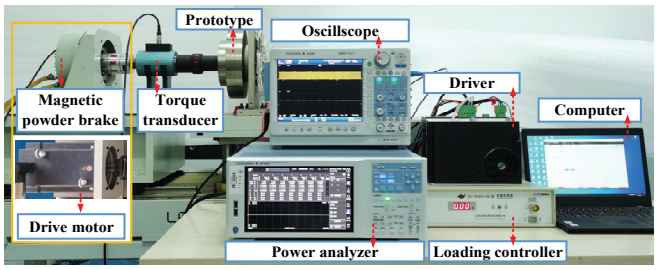

Fig. 16. Prototype testing platform.

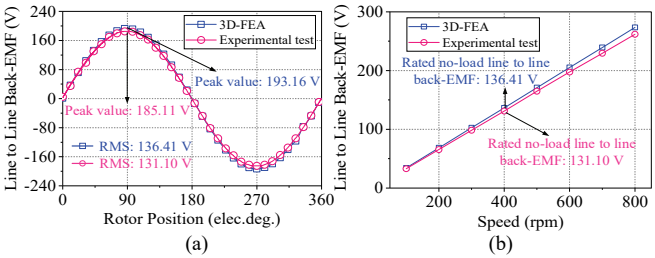

Fig. 17. No-load line to line back-EMF performances of the EDTW-DRSAFPM machine. (a) Rated speed condition. (b) Variation against speed.

The no-load line to line back-EMF of the prototype is measured, which is shown in Fig. 17. It can be seen that the RMS of the rated no-load line to line back-EMF of the experimental test (131.10 V) agrees well with that of the 3D-FEA (136.41 V), with an error of 3.89 %, which validates the feasibility of the proposed machine and the correctness of the analysis mentioned above. The no-load line to line back-EMF variation against speed of the prototype is shown in Fig. 17(b). As can be seen, within the whole speed range, the RMS of the

This article has been accepted for publication in a future issue of this journal, but has not been fully edited. Content may change prior to final publication. Citation information: DOI 10.1109/TIE.2022.3159956, IEEE Transactions on Industrial Electronics

line to line back-EMF of the experimental test matches well with that of the 3D-FEA.

Fig. 18 presents the simulated and measured three-phase current of the prototype at the rated state. The experimental conditions are that the prototype operates at (400 rpm) rated speed, the loading controller is used to adjust the load of the magnetic powder brake, the current is measured by power analyzer and extracted when the current reaches the rated value (10 A rms) by adjusting the load of the magnetic powder brake. Fig. 19 shows the output torque of the prototype. It is shown that the average torque of the experimental test is 53.74 Nm, which is 4.78 % lower than that of the 3D-FEA (56.44 Nm). In addition, the torque ripple of the 3D-FEA and experimental test are 3.32 % and 3.62 %, respectively. The torque-current characteristic of the prototype is presented in Fig. 19(b). It is shown that the trends of output torque versus current of the experimental test and the 3D-FEA are basically consistent, with an 3.45 % average error. In conclusion, the results of the experimental test match well with that of the 3D-FEA under no-load and on-load conditions, which validate the feasibility of the DRSAFPM machine with EDTW and the correctness of the 3D-FEA. The reasons for the slight errors between the results of the 3D-FEA and experimental test are that the manufacture error and the neglect of the mechanical loss of the 3D-FEA.

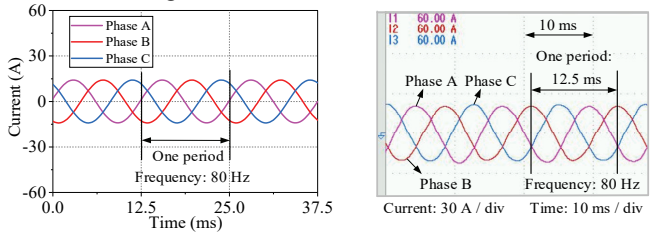

(a) (b)

Fig. 18. The simulated and measured three-phase current of the prototype at rated state. (a) Simulated current. (b) Measured current.

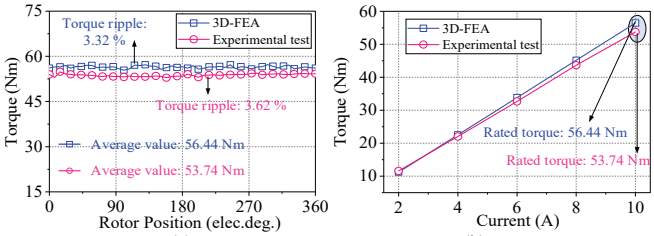

(a) (b)

Fig. 19. Output torque of the EDTW-DRSAFPM machine. (a) Rated current condition. (b) Variation against current.

VI. Conclusion and Discussion

Based on the analysis and comparison of the DRSAFPM machines with conventional CWs and those with EDTW in coil layout, EMF, winding MMF, coil factor, size equations and electromagnetic performance, there are some conclusions which could be summarized as follows:

1) Different from the DRSAFPM machines with conventional CWs, it can be concluded that the pitch factor of the DRSAFPM machine with EDTW is always 0.5. The magnitude of the coil factor of the EDTW-DRSAFPM machine is only determined by the band factor. In addition, the number of turns per phase N_{ph} of the EDTW-DRSAFPM machine is twice that of the DRSAFPM machines with conventional CWs, when the number of conductors per phase N_c of the DRSAFPM machines with conventional CWs and EDTW are identical. Therefore, it is necessary to introduce the conductor factor K_{c2} to represent the back-EMF capability of the DRSAFPM machines with conventional CWs and EDTW.
2) Thanks to the high conductor factor K_{c2} of the EDTW-DRSAFPM machine, it has superiority in back-EMF amplitude and torque density than the DRSAFPM machines with conventional CWs (when their N_c is similar). The simulation result shows that the electromagnetic torque of the EDTW-DRSAFPM machine is 12.59 % and 47.23 % higher than that of the SLCW- and DLCW-DRSAFPM machines. The prototype of the EDTW-DRSAFPM machine is manufactured and tested. The results of the experimental test under no-load and on-load conditions match well with that of the simulation, which validate the feasibility of the proposed machine and the correctness of the 3D-FEA. The slight errors between the simulation and experimental test are caused by the manufacturing error and the neglect of the mechanical loss in simulation. Such EDTW-DRSAFPM machines are suitable for low-speed and high torque applications.
3) This paper is focus on the slotless and surface mounted AFPM machine with EDTW. To further improve the torque density, strengthen flux-weakening ability and extend speed range, the slotted and interior AFPM machine with EDTW will be studied in the following research.

References

[1] M. Q. Wang, C. D. Tong, Z. Y. Song, J. Q. Liu, and P. Zheng, "Performance analysis of an axial magnetic-field-modulated brushless double-rotor machine for hybrid electric vehicles," *IEEE Trans. Ind. Electron.*, vol. 66, no. 1, pp. 806-817, Jan. 2019.

[2] P. Virtič, M. Vražić, and G. Papa, "Design of an axial flux permanent magnet synchronous machine using analytical method and evolutionary optimization," *IEEE Trans. Energy Convers.*, vol. 31, no. 1, Mar. 2016.

[3] B. C. Guo, Y. K. Huang, F. Peng, J. N. Dong, and Y. J. Li, "Analytical modeling of misalignment in axial flux permanent magnet machine," *IEEE Trans. Ind. Electron.*, vol. 67, no. 6, Jun. 2020.

[4] W. M. Tong, S. Wang, S. H. Dai, S. N. Wu, and R. Y. Tang, "A quasi-three-dimensional magnetic equivalent circuit model of a double-sided axial flux permanent magnet machines considering local saturation," *IEEE Trans. Energy Convers.*, vol. 33, no. 4, pp. 2163-2173, Dec. 2018.

[5] F. G. Capponi, G. D. Donato, and F. Caricchi, "Recent advances in axial-flux permanent-magnet machine technology," *IEEE Trans. Ind. Appl.*, vol. 48, no. 6, pp. 2190-2205, Nov./Dec. 2012.

[6] M. Aydin, S. R. Huang, and T. A. Lipo, "Torque quality and comparison of internal and external rotor axial flux surface-magnet disc machines," *IEEE Trans. Ind. Electron.*, vol. 53, no. 3, pp. 822-830, Jun. 2006.

[7] R. Wilson, R. Gandhi, A. Kumer, and R. Roy, "Performance analysis of twin-rotor axial flux permanent magnet synchronous motor for in-wheel electric vehicle applications with sensorless optimized vector control strategy," in *IEEE International Conference on Power Electronics, Drives and Energy System (PEDES)*, Jaipur, India, Dec. 2020.

[8] M. Aydin, and M. Gulec, "A new coreless axial flux interior permanent magnet synchronous motor with sinusoidal rotor segments," *IEEE Trans. Magn.*, vol. 52, no. 7, Art. ID. 8105204, Jul. 2016.

[9] Z. R. Zhang, C. Wang, W. W. Geng, "Design and optimization of Halbach-array PM rotor for high-speed axial-flux permanent magnet machine with ironless stator," *IEEE Trans. Ind. Electron.*, vol. 67, no. 9, pp. 7269-7279, Sep. 2020.

[10] T. J. Woolmer, and M. D. Mcculloch, "Analysis of the yokeless and segmented armature machine," in *IEEE International Electric Machines & Drives Conference*, Antalya, Turkey, Jul. 2007.

[11] B. Zhang, T. Seidler, R. Dierken, and M. Doppelbauer, "Development of a yokeless and segmented armature axial flux machine," *IEEE Trans. Ind. Electron.*, vol. 63, no. 4, pp. 2062-2071, Apr. 2016.

[12] J. J. Chang, Y. N. Fan, J. L. Wu, and B. Zhu, "A yokeless and segmented armature axial flux machine with novel cooling system for in-wheel traction applications,' *IEEE Trans. Ind. Electron.*, vol. 68, no. 5, pp. 4131-4140, May. 2021.
[13] D. Winterborne, N. Stannard, L. Sjoberg, and G. Atkinson, "An air-cooled YASA motor for in-wheel electric vehicle applications,' *IEEE Trans. Ind. Appl.*, vol. 56, no. 6, pp. 6448-6455, Nov./Dec. 2020.
[14] W. Jara, P. Lindh, J. A. Tapia, *et al*., "Rotor eddy-current losses reduction in an axial flux permanent-magnet machine," *IEEE Trans. Ind. Electron.*, vol. 63, no. 8, pp. 4729-4737, Aug. 2016.
[15] G. D. Donato, F. G. Capponi, and F. Caricchi, "Fractional-slot concentrated-winding axial-flux permanent-magnet machine with core-wound coils," *IEEE Trans. Ind. Appl.*, vol. 48, no. 2, pp. 630-641, Mar./Apr. 2012.
[16] F. G. Capponi, G. D. Donato, G. A. Rivellini, and F. Caricchi, "Fractional-slot concentrated-winding axial-flux permanent-magnet machine with tooth-wound coils,' *IEEE Trans. Ind. Appl.*, vol. 50, no. 4, pp. 2446-2457, Jul./Aug. 2014.
[17] C. X. Gao, M. Z. Gao, J. K. Si, H. C. Feng, and W. P. Cao, "A novel direct-drive permanent magnet synchronous motor with toroidal windings," *Energies*, vol. 12, no. 3, Art. ID. 432, Feb. 2019.
[18] Y. Q. Wei, J. K. Si, Z. P. Cheng, *et al.*, "Design and characteristic analysis of a six-phase direct-drive permanent magnet synchronous motor with 60deg phase-belt toroidal winding configuration for electric vehicle," *IET Elec. Power Appl.*, vol. 14, no. 13, pp. 2659-2666, Dec. 2020.
[19] H. Y. Lee, E. C. Lee, S. O. Kwon, and J. P. Hong, "A study on brushless PM slotless motor with toroidal winding," in *IEEE International Electric Machine and Drives Conference*, Miami, FL, USA, 2017.
[20] H. N. Phyu, N. L. H. Aung, and C. Bi, "Influence of winding structure and the effect of MMF harmonics to the spindle motor performance for ultrahigh TPI HDD," *IEEE Trans. Magn*., vol. 49, no. 6, pp. 2776-2781, Jun. 2013.
[21] B. Xia, J. X. Shen, P. C. K. Luk, and W. Z. Fei, "Comparative study of air-cored axial-flux permanent-magnet machines with different stator winding configurations," *IEEE Trans. Ind. Electron.*, vol. 62, no. 2, pp. 846-856, Feb. 2015.
[22] S. R. Huang, J. Luo, F. Leonardi, and T. A. Lipo, "A comparison of power density for axial flux machines based on general purpose sizing equations," *IEEE Trans. Energy Convers*., vol. 14, no. 2, pp. 185-192, Jun. 1999.
[23] J. F. Gieras, R. -J. Wang, and M. Kamper, Axial flux permanent magnet brushless machines, 2nd ed. New York: Springer-Verlag, 2008.
[24] A. Hemeida, M. Taha, A. A.-E. Abdallh, *et al*., "Applicability of fractional slot axial flux permanent magnet synchronous machines in the field weakening region," *IEEE Trans. Energy Convers*., vol. 32, no. 1, pp. 111-121, Mar. 2017.
[25] A. M. EL-Refaie, and T. M. Jahns, "Optimal flux weakening in surface PM machines using fractional-slot concentrated windings," *IEEE Trans. Ind. Appl.*, vol. 41, no. 3, pp. 790-800, May/Jun. 2005.

Jikai Si (M'20) received the B.S. degree in electrical engineering and automation from the Jiaozuo Institute of Technology, Jiaozuo, China, in 1998; the M.S. degree in electrical engineering from Henan Polytechnic University, Jiaozuo, China, in 2005; and the Ph.D. degree in 2008 from the School of Information and Electrical Engineering, China University of Mining and Technology, Xuzhou, China, in 2008.

He is currently a distinguished professor at Zhengzhou University. His main research interests include the theory, application, and control of special motor. He has authored and co-authored over 160 technical papers in these areas. Prof. Si is a Member of the Green Motor System Professional Committee, China.

Tianxiang Zhang was born in Nanyang, Henan, China in 1997. He received the B.S. degree in electrical engineering from Zhengzhou University of Light Industry, Zhengzhou, in 2019. He is currently working torward the M.S. degree in School of Electrical Engineering of Zhengzhou University, Zhengzhou, Henan.

His research interests include design, analysis and control of axial-flux permanent magnet motors.

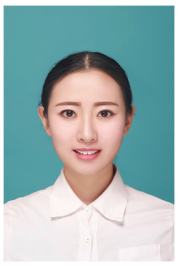

Rui Nie received B.S. degree in electrical engineering from Henan Polytechnic University, Jiaozuo, China, in 2015, and Ph.D. degree in electrical engineering from the China University of Mining and Technology, Xuzhou, China, in 2020. She is currently doing post-doctral research at Zhenzhou University.

Her current research interests include linear motor design and control, and renewable energy generation technology.

Chun Gan (M'14) received the Ph.D. degree in electrical engineering and motor drives from Zhejiang University, Hangzhou, China, in 2016.

He is currently a Professor with the School of Electrical and Electronic Engineering, Huazhong University of Science and Technology, Wuhan, China. His research interests include electrical motor drives, electrical motor design, electric vehicles, hybrid vehicles, and high-efficiency power converters His current research interests include the theory, application, and control of special motor and power electronics.

Yihua Hu (M'13-SM'15) received the B.S. degree in electrical motor drives, in 2003, and the Ph.D. degree in power electronics and drives, in 2011, both from China University of Mining and Technology, Jiangsu, China. Between 2011 and 2013, he was a Postdoctoral Fellow with the College of Electrical Engineering, Zhejiang University, Zhejiang, China.

He is currently a distinguished professor at University of York. His research interests include PV generation system, power electronics converters and control, and electrical motor drives.